SCIENTIFIC REPORTS

OPEN

SUBJECT AREAS:
SYNTHESIS AND PROCESSING
SPINTRONICS
SURFACES, INTERFACES AND THIN FILMS
MAGNETIC PROPERTIES AND MATERIALS

Received
11 September 2014

Accepted
8 December 2014

Published
19 January 2015

Correspondence and requests for materials should be addressed to Q.L.M. (qinli-ma@wpi-aimr.tohoku.ac.jp)

Artificially engineered Heusler ferrimagnetic superlattice exhibiting perpendicular magnetic anisotropy

Q. L. Ma, X. M. Zhang, T. Miyazaki & S. Mizukami

World Premier International Research Center, Advanced Institute for Materials Research, Tohoku University, 2-1-1, Katahira, Sendai, 980-8577, Japan.

To extend density limits in magnetic recording industry, two separate strategies were developed to build the storage bit in last decade, introduction of perpendicular magnetic anisotropy (PMA) and adoption of ferrimagnetism/antiferromagnetism. Meanwhile, these properties significantly improve device performance, such as reducing spin-transfer torque energy consumption and decreasing signal-amplitude-loss. However, materials combining PMA and antiferromagnetism rather than transition-metal/rare-earth system were rarely developed. Here, we develop a new type of ferrimagnetic superlattice exhibiting PMA based on abundant Heusler alloy families. The superlattice is formed by [MnGa/Co_2FeAl] unit with their magnetizations antiparallel aligned. The effective anisotropy (K_u^{eff}) over 6 Merg/cm^3 is obtained, and the SL can be easily built on various substrates with flexible lattice constants. The coercive force, saturation magnetization and K_u^{eff} of SLs are highly controllable by varying the thickness of MnGa and Co_2FeAl layers. The SLs will supply a new choice for magnetic recording and spintronics memory application such as magnetic random access memory.

Nanometer ferromagnets have been widely used in storage media[1–6], non-volatile memory and logical devices based on spintronics, where the magnetization is manipulated by magnetic field[7–11], spin-polarized current[12,13], and electric field[14,15]. As demanded by cell minimization, ferromagnets employed for information storage experienced a transition from in-plane to perpendicular magnetization in last decades. Several types of ferromagnets with perpendicular magnetic anisotropy (PMA) were developed to fulfill this request, including tradition/noble metal alloys/multilayers (e.g, FePt, CoPt alloys), rare-earth/transition metal alloys[16], newly developed CoFeB thin films[17], and recent promising tetragonal Heusler alloys[18–20]. The high K_u^{eff} is necessary to overcome the thermal fluctuation as cell lateral size minimization. Additional advantages are the low energy consumption of the spintronics-devices manipulated by spin-transfer torque (STT) and the simplified head structure for Hard disk drive storage. Beyond the stability requested for individual cells, the long-range static magnetic interaction between neighboring magnetic units becomes critically important as the density increasing when facing the integration of devices. As the bit distance decreases, a collective behavior occurs as a result of the dipolar interaction[21–23]. Ferrimagnetic/antiferromagnetic materials were proposed as recording media, owing to the fact that the distance between ferrimagnetic especially antiferromagnetic islands can be drastically reduced without fearing of the information stored on one island affecting that of neighboring islands compared to ferromagnets. In addition, the antiferromagnetic bit has a low signal amplitude loss compared with usual ferromagnets[6]. Beyond being proposed for recording media, antiferromagnetic and ferrimagnetic composites have drawn intensive attention recently, owing to their abundant domain phase-diagram[24,25], special dynamics process and unusual FMR model[26–30]. In addition, the double magnetic sub-lattice makes them one of the candidate for all optical switching media[31–35]. Nowadays, the perpendicular magnetized ferromagnetic composite were mainly based on transition-metal/rare-earth system, such as Dy-Co and Tb-Fe alloy/multilayers, and ferromagnetic/nonmagnetic multilayers with interlayer antiferromagnetic coupling[34–37]. However, the fabrication and investigation on perpendicularly magnetized ferrimagnetic composites based on 3*d* metal without noble and rare-earth elements is rarely been reported, owing to the significant challenge of developing easily-to-built ferrimagnetic composites with systematically controllable parameters.

Here, using the Heusler alloys $Mn_{62}Ga_{38}$ (MnGa) and $Co_{50}Fe_{23.7}Al_{26.3}$ (CFA), we design a new ferrimagnetic superlattices (SLs) exhibiting PMA for magnetic recording and spintronics devices application. The MnGa and CFA alloys used for SLs architecture are $L1_0$ ordered PMA ferromagnet and cubic soft ferromagnet, respect-

ively[18,38], ensuring that the magnetic parameters of SLs formed with [MnGa/CFA] are highly flexible. Both of the alloys belong to the Heusler family with small in-plan lattice mismatch, which makes the architecture of SLs available with tunable lattice constants. Ideal Co_2FeAl, shown in Figure 1a, has an $L2_1$ structure, where Fe and Al atoms occupy two interpenetrating fcc lattices with an NaCl-type structure[33]. The Co atoms form a simple cubic lattice, and they are tetrahedrally coordinated with both the Fe and Co atoms, at the corners of a cube. Mn_xGa_{100-x} is a promising tetragonal Heusler alloy exhibiting PMA[18–20]. The $L1_0$ structure stable for x = 50–65, is a highly distorted tetragonal variant of the $L2_1$ Heusler unit cell, which is stretched by ~25% along the *c* axis. The structure of $Mn_{50}Ga_{50}$ can be regarded as periodic atomic planes of Mn and Ga along the *c* direction. As the Mn content increases, parts of the Ga atoms are replaced by Mn atoms, and the moments of the substituted Mn atoms are antiparallel to those of the original Mn atoms along the *c* direction[20].

Results

Ordered structure with flexible lattice constants of SLs. The periodic layered SLs illustrated in Figure 1b are formed by [MnGa/CFA] units with the magnetizations of the MnGa and CFA layers antiparallel to each other owing to the antiferromagnetic interfacial exchange coupling between them. Figure 1c shows the typical transmission electron microscope (TEM) cross-sectional image of $[MnGa(3.0\ nm)/CFA(1.5\ nm)]_5$ SL deposited on an MgO(001) single-crystal substrate buffered with a 40-nm-Cr layer. Well crystallized structure is shown in the sample, where the MnGa and CFA layers have the same in-plane lattice constant, indicated by the continuous vertical lattice line. The clear alternative Energy Dispersive X-ray (EDX) spectroscopy peaks of Mn (MnGa) and Co (CFA) shown in Figure 1d indicate the periodic layered structure formed in the SL sample.

To study the structure and magnetic properties systematically, four series of SLs with different thickness of CFA (t_{CFA} = 0.5, 1.0, 1.5, and 2.0 nm) were fabricated on MgO(001) substrate, which are denoted as CFA05, CFA10, CFA15 and CFA20, respectively. The thickness of the MnGa layer (t_{MnGa}) in each series varies from 1.0 to 6.0 nm (see method). The lattice parameters of the SLs were determined by in-plane and out-of-plane X-ray diffraction (XRD) using a Cu K_α source with λ = 1.5418 Å. Figure 2a shows the in-plane 2θ patterns of the CFA05 samples. The single (200) peaks indicate the same in-plane lattice constant (*a*) for MnGa and CFA in each sample, which is consistent with the TEM result. As t_{MnGa} increases, diffraction peaks of SLs shift to higher angle gradually, implying that the *a* value decreases as t_{MnGa} increases. The out-of-plane 2θ patterns of CFA05 SLs are shown in Figure 2b. The (004) peaks of SLs marked in the square shift from 61.81° to 51.75° gradually, corresponding to the increase in lattice constant *c* of the SLs as t_{MnGa} increases. The diffraction peaks of (200) and (004) of SLs shown in Figures (a) and (b) indicates well-ordered structure formed in SLs, where MnGa and CFA layers have $L1_0$ and B_2 ordering[20,38]. Detailed XRD patterns of all SL samples are shown in supporting information (Figures S1 to S5).

Owing to the in-plane lattice mismatch between the MnGa and CFA materials, the lattice constants of SLs strongly depend on the thickness of the MnGa and CFA layers. The *a* and *c* values of SLs calculated from the XRD patterns are summarized in Figures 2c and d, respectively. Generally, the SLs lattice exhibits a transition from CFA-dominated to MnGa-dominated as t_{MnGa} increase for each series. Here, the *a* values of SLs are calculated in the frame of tetragonal cell as a reference of MnGa cell, where *a* is $\sqrt{2}/2$ times of the cubic cell (*a*'). For each series, *a* decreases as t_{MnGa} increases and exhibits a dramatic change at certain t_{MnGa}, which possibly correspond to the transition of the SLs from cubic to tetragonal. The *c* values of SLs exhibit a monotonic increase with t_{MnGa} in each series and SLs with thinner t_{CFA} have larger *c*. As the MnGa layer is thick enough, such as 4 and 6 nm for the CFA05 and CFA15 series, the *c* of SLs are almost same as that of the MnGa alloys.

Ferrimagnetism and PMA nature of SLs with widely tunable parameters. Typical *M*(*H*) loops in the perpendicular direction for CFA15 SLs are plotted in Figure 3a. For $t_{MnGa} \geq 2.0$ nm, the SLs exhibits PMA indicated by square-shaped *M*(*H*) loops. It is noted that both the H_c and M_s of SLs strongly depend on t_{MnGa}, and exhibit a non-monotonic dependence. The perpendicular *M*(*H*) loops of the

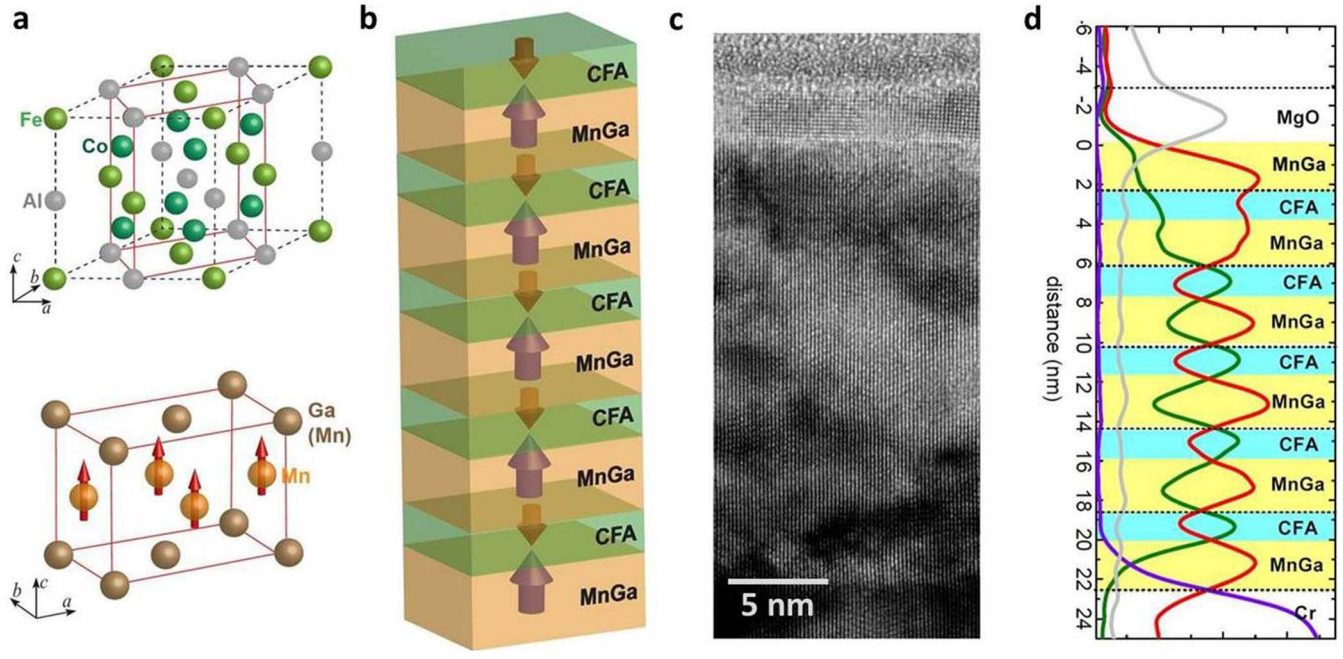

Figure 1 | Formation and structural information of SLs. (a), Schematic picture of $L2_1$ Co_2FeAl (up) and $L1_0$ MnGa (down) alloys. (b), Illustration of ferrimagnetic SLs, where the magnetizations of the CFA and MnGa layers are antiparallel aligned. (c), (d), Cross-sectional TEM image (c) and EDX spectrum (d) of $[MnGa(1.5\ nm)/CFA(3\ nm)]_5$ SL on an MgO(001) substrate. The gray, red, green and purple lines in (d) correspond to the EDX intensity of the Mg, Mn, Co, and Cr elements, which correspond to the MgO, MnGa, CFA and Cr layers, respectively.

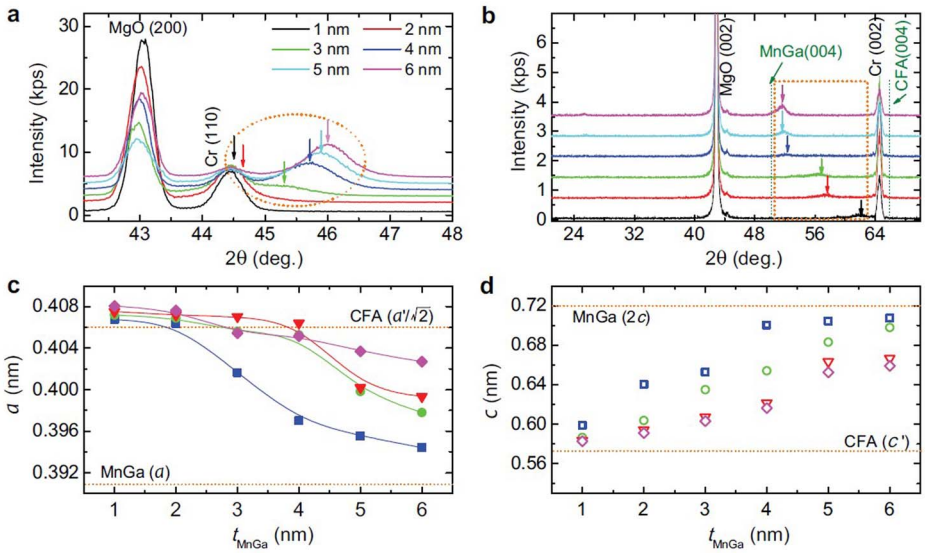

Figure 2 | XRD patterns and lattice constants of SLs on MgO(001) substrate. (a),(b), In-plane (a) and out-of-plane (b) XRD patterns for [MnGa(t_{MnGa} nm)/CFA(0.5 nm)]5, where t_{MnGa} = 1, 2, 3, 4, 5, and 6 nm. The green dotted lines in (b) are typical 004 peak positions for MnGa and CFA bulk materials. The diffraction pattern of (200) and (004) peaks are marked in the dashed circles in (a) and (b), respectively. (c), (d), Lattice constant a (c) and c (d) as a function of t_{MnGa} for four SL series, where t_{CFA} = 0.5 (squares), 1 (circles), 1.5 (triangles), and 2.0 nm (diamonds). As t_{MnGa} increases, the lattice constants change gradually from CFA-regime to MnGa-regime, which are marked with dashed lines.

four series of SLs are shown in supporting information (Figures S6 to S9). Figure 3b shows the perpendicular and in-plane $M(H)$ loops for the [MnGa(6 nm)/CFA(1.5 nm)]$_5$ sample. A linear $M(H)$ loop in the in-plane direction indicates a well PMA, and the effective anisotropy (K_u^{eff}) calculated from $H_sM_s/2$ is 6.8 Merg/cm^3, where H_s is the saturation field of the in-plane $M(H)$ curve.

The M_s of SLs as a function of t'_{MnGa} (t'_{MnGa} is effective thickness of MnGa layer with consideration of additional MnGa layer on the top of SLs, see method) for the four SL series are shown in Figure 3c. For each series, M_s firstly decreases in the CFA-dominated regime as t_{MnGa} increases, owing to the fact that the increase in the antiparallel-aligned magnetization of MnGa decreases the net magnetization of SLs. As t'_{MnGa} increases further in the MnGa-dominated regime, M_s increases as t'_{MnGa} increases, owing to the magnetization of SLs being in the same direction as the MnGa layers. Based on the antiparallel alignment of magnetizations of MnGa and CFA layers, the M_s of SLs can be described by the following formula.

$$M_s = \left|(M_{MnGa}t'_{MnGa} - M_{CFA}t_{CFA})/(t'_{MnGa} + t_{CFA})\right| \quad (1)$$

The fits are shown by the solid lines in Figure 3c; the fitted magnetizations of the MnGa and CFA layers are ~460 and ~1050 emu/cm^3, respectively, which are comparable to the values of bulk MnGa and CFA materials[18,38] (see supporting information Figure S10). It is noted that, the magnetization of SLs is zero for certain t'_{MnGa}, so-called compensational points. At these points, the magnetizations of

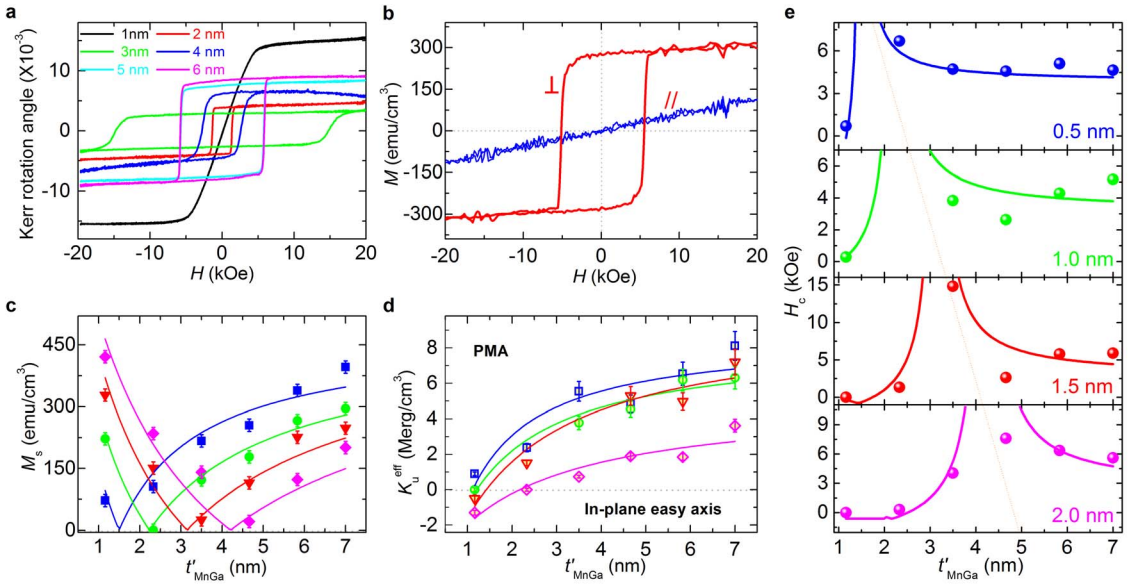

Figure 3 | Magnetic properties of SLs on MgO(001) substrate. (a), Out-of-plane Kerr loops of the CFA15 series. (b), Out-of-plane (⊥) and in-plane (//) $M(H)$ loops of the [MnGa(6.0 nm)/CFA(1.5 nm)]$_5$ SL. (c), (d), (e), M_s (c), K_u^{eff} (d) and H_c (e) of SLs as a function of t'_{MnGa} for the CFA05, CFA10, CFA15 and CFA20 series, where t_{CFA} = 0.5 (squares), 1.0 (circles), 1.5 (triangles), and 2.0 nm (diamonds). t'_{MnGa} is effective MnGa thickness with consideration of addtional MnGa layer deposited on the top of SLs. The solid lines in c, d and e are fits based on formulas (1), (2) and (3), respectively.

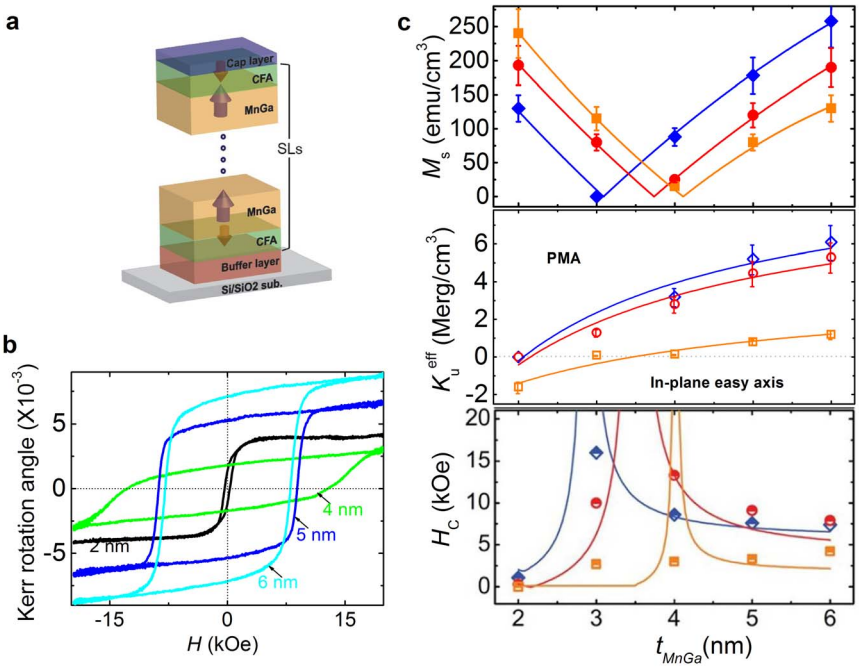

Figure 4 | Fabrication of SLs on SiO_2 amorphous substrate. (a), SL film stack structure deposited on the Si/SiO_2 substrate. (b), Out-of-plane Kerr loops of the cfa15 series, where t_{CFA} = 1.5 nm. The black, green, blue and cyan lines are the Kerr loops of SLs with t_{MnGa} = 2, 4, 5, and 6 nm, respectively. (c), M_s, H_c and K_u^{eff} of SLs as a function of t_{MnGa} for the cfa12, cfa15, cfa20 series, where t_{CFA} = 0.5 (diamonds), 1.0 (circles), and 1.5 nm (squares). The solid lines in each panel are fits based on formula (1), (2) and (3), respectively.

the CFA and MnGa layers have the same magnitude with antiparallel configuration, the SLs are antiferromagnetic composites.

K_u^{eff} of the SLs estimated from $H_sM_s/2$ are plotted in Figure 3d. Generally, SLs with small t_{CFA} and large t'_{MnGa} exhibit a high K_u^{eff}; the phase-diagram of K_u^{eff} as a function of t_{CFA} and t'_{MnGa} is shown in the supporting information (Figure S11). For a density of 1 Tbit/inch^2, the smallest volume V for the stability condition $K_u^{eff}V/k_BT \geq 60$ to be satisfied at room temperature is 800 nm^3 if considering the distance between neighboring bits is the same as the bit diameter, for K_u^{eff} of 3 Merg/cm^3. This volume corresponds to a nano-pillar with a height equal to its diameter with dimensions of 10.5 nm[17]. Assume the PMA of SLs originates from the MnGa layers, the K_u^{eff} the of SLs can be described by:

$$K_u^{eff} = (K_{u-MnGa}t'_{MnGa} - 2\pi M_{CFA}{}^2 t_{CFA})/(t_{CFA} + t'_{MnGa}) \quad (2)$$

where $K_{u\text{-}MnGa}$ denotes the effective uniaxial anisotropy of the MnGa layer in SLs. From the fits shown with the solid lines, the $K_{u\text{-}MnGa}$ and M_{CFA} are ~8 Merg/cm^3 and ~1100 emu/cm^3, respectively (see support information Fig. S12). It is reasonable to attribute the smaller $K_{u\text{-}MnGa}$ compared with the bulk material to the structural change of the MnGa layer in SLs. In particular, the $K_{u\text{-}MnGa}$ is 6 Merg/cm^3 for the CFA20 series owing to the cubic-like lattice of the SLs.

In each series, H_c shows a maximum value near compensational points marked by the dotted line in Figure 3e. H_c decreases to zero as t_{MnGa} decrease to zero, where the PMA of SLs disappears. On the other side, H_c saturates to that of single-MnGa-layer when t'_{MnGa} is thick enough, where the property of SLs is dominated by the MnGa. Here, simply based on the Stoner-Wohlfarth description, the coercivity is proportional to the uniaxial anisotropy field[39]

$$H_c = 2C\ K_u^{eff}/M_s. \quad (3)$$

Thus, H_c increases as the magnetization decreases for certain K_u^{eff}. In principle, H_c is infinite at the compensational points. The solid-lines in Figure 3e are the fitted values from 2C K_u^{eff}/M_s, with the scaling factor C is around 0.1. Ideally, the constant C is 1 for single domain particles. The small scaling factor in the fitting is because the H_c of continuous film depend on nucleation field, in addition to K_u^{eff} only. It shows that the non-monotonic t'_{MnGa} dependent of H_c can be well described by the Stoner-Wohlfarth model[39].

Formation of SLs on SiO_2 amorphous substrate. For materials designed for application, fabrication on different substrates, especially on amorphous substrates, is essentially important. Here, we demonstrate the formation of textured SLs on an amorphous substrate. The SL stacks with periodic CFA/MnGa layers were deposited on Si/SiO_2 substrate at room temperature, buffered with Ta(10 nm)/Cr(5 nm)/MgO(2 nm) and capped with 5-nm-Ta layer, as shown in Figure 4a. Post annealing at 400°C was performed for 10 min in vacuum to crystallize the SLs. Three series of SLs (cfa12, cfa15 and cfa20) were fabricated, where t_{CFA} = 1.2, 1.5, and 2.0 nm, respectively. Square-shaped out-of-plane $M(H)$ loops of cfa15 SLs are observed, as shown in Figure 4b. This indicates that the SLs exhibit PMA owing to the textured structure formed on SiO_2 substrate. Up to now, tetragonal MnGa layers were only achieved on single crystal substrates such as GaAs(001) $SiTiO_3$(001) and MgO(001) owing to the matastable nature of the tetragonal order[40–42]. The ordered structure of SLs well formed on the amorphous substrate is likely induced by the crystalline structure of the CFA layer. The t_{MnGa} dependence of M_s, K_u^{eff} and H_c of the SLs for the three series are summarized in Figure 4c, where the solid lines are the fits based on formula (1), (2), and (3), respectively. The M_{MnGa} and M_{CFA} in these SLs from the fit of $M_s(t_{MnGa})$ are ~460 and ~1100 emu/cm^3, which is consistent with that for the SLs deposited on MgO(001) substrate.

Discussion

The magnetism of Mn-Ga alloys originates from the Mn atoms, which have a half-filled d shell. This makes the exchange interaction involving Mn-Ga thin film more sensitive to the interfacial environment and more flexible to being tuned. An antiferromagnetic exchange coupling at the MnGa/Co_2FeAl interface was achieved when the structure was annealed at 400°C, owing to the Co atoms

presented in the interface[43]. Since both the materials belong to the Heusler family, this supplies the structural basis for the architecture of the ferrimagnetic SL. The in-plane lattice mismatch and different magnetic properties of MnGa and CFA enable well control of the properties of SLs by simply changing the thickness of MnGa and CFA layers. The SLs depicted here, can be easily built on amophous substrates, exhibit flexible magnetic and structure properties, leading to a desirable combination for wide applictions in information storage.

In summary, based on antiferromagnetic exchange coupling at the MnGa/CFA interface, we developed ferrimagnetic SLs exhibiting high PMA with K_u^{eff} over 6 Merg/cm^3. The SLs formed with [MnGa(t_{MnGa})/CFA(t_{CFA})] units exhibit widely tunable magnetic properties, with M_s and H_c varying from 0 to 400 emu/cm^3, and from 30 mT to 1500 mT. At the compensation points, where the antiparallel aligned magnetizations of MnGa and CFA have same magnitude, the SLs are antiferromagnets exhibiting zero M_s with PMA, which is a potential candidate for antiferromagnetic electronics and all-optical switching media.

Experimental section

Sample preparation. The stoichiometric compositions of the Co_2FeAl and Mn-Ga films were $Co_{50}Fe_{23.7}Al_{26.3}$ (CFA) and $Mn_{62}Ga_{38}$ (MnGa), analyzed with inductively coupled plasma mass spectrometry. [MnGa(t_{MnGa})/CFA(t_{CFA})]$_5$/MnGa(t_{MnGa}) SL stacks were fabricated using an ultrahigh-vacuum sputtering system with a base pressure of less than 1×10^{-7} Pa on a MgO(001) single-crystal substrate, with a 40-nm-Cr as the buffer layer. Here, t_{MnGa} = 1.0, 2.0, 3.0, 4.0, 5.0 and 6.0 nm, t_{CFA} = 0.5, 1.0, 1.5, and 2.0 nm. Since there is an additional MnGa layer on the 5-periodic MnGa/CFA structure, the effective MnGa thickness (t'_{MnGa}) is in the used in the discussion of magnetic properties, where $t'_{MnGa} = 6t_{MnGa}/5$. All of the layers were deposited at room temperature and in-situ annealing was carried out at 700°C after the deposition of Cr. Then, a capping layer of MgO(2.2 nm)/Ta(2.0 nm) was deposited on top to prevent contamination and oxidation of the SLs. The SLs deposited on the SiO_2 substrate were fabricated under the same conditions with a buffer layer of Ta(5.0 nm)/Cr(5.0 nm)/MgO(2.0 nm). Three series of SLs were fabricated on the SiO_2 substrate with structure of [MnGa(t_{MnGa})/CFA(t_{CFA})]$_5$, where t_{CFA} = 1.2, 1.5 and 2.0 nm. In each series, t_{MnGa} varies from 2.0 to 6.0 nm. Before the measurement, the SLs stacks were annealed for 10 min at 400°C in vacuum.

Characterization. The crystal structure was characterized using XRD both in-plane and out-of-plane with a 9-kW rotating anode. The Cu K_α line (wave length λ = 1.5418 Å) was used in the experiment. Atomic structure was characterized using high-resolution TEM (HRTEM) with an accelerate voltage of 200 kV. The element distribution was examined using EDX spectroscopy. The magnetic properties were measured using a vibrating sample magnetometer and the polar magneto-optical Kerr effect at room temperature with a field range of 2 T.

1. Iwasaki, S. & Nakamura, Y. An analysis for the magnetization mode for high density magnetic recording. *IEEE Trans. Magn.* **MAG-13**, 1272–1277 (1977).
2. Park, B. G. *et al.* A spin-valve-like magnetoresistance of an antiferromagnet-based tunnel junction. *Nat. Mater.* **10**, 347–351 (2011).
3. Loth, S. Bistability in Atomic-Scale Antiferromagnets. *Science* **335**, 196–199 (2012).
4. Acharya, B. R., Abarra, E. N. & Okamoto, I. SNR Improvements for Advanced Longitudinal Recording Media. *IEEE Trans. Magn.* **37**, 1475–1477 (2001).
5. Mangin, S. *et al.* Current-induced magnetization reversal in nanopillars with perpendicular anisotropy. *Nat. Mater.* **5**, 210–215 (2006).
6. Fullerton, Eric, E. *et al.* Antiferromagnetically coupled magnetic media layers for thermally stable high-density recording. *Appl. Phys. Lett.* **77**, 3806–3808 (2000).
7. Chou, S. Y. *et al.* Single-domain magnetic pillar array of 35 nm diameter and 65 Gbits/in.^{2} density for ultrahigh density quantum magnetic storage. *J. Appl. Phys.* **76**, 6673–6675 (1994).
8. Miyazaki, T. & Tezuka, N. Giant magnetic tunneling effect in Fe/Al_2O_3/Fe junction. *J. Magn. Magn. Mater.* **139**, L231–L234 (1995).
9. Moodera, J. S. *et al.* Large Magnetoresistance at Room Temperature in Ferromagnetic Thin Film Tunnel Junctions. *Phys. Rev. Lett.* **74**, 3273–3276 (1995).
10. Parkin, S. S. P. *et al.* Giant tunnelling magnetoresistance at room temperature with MgO (100) tunnel barriers. *Nat. Mater.* **3**, 862–867 (2004).
11. Yuasa, S. *et al.* Giant room-temperature magnetoresistance in single-crystal Fe/MgO/Fe magnetic tunnel junctions. *Nat. Mater.* **3**, 868–871 (2004).
12. Slonczewski, J. Current-driven excitation of magnetic multilayers. *J. Magn. Magn. Mat.* **159**, L1–L7 (1996).
13. Krivorotov, I. V. *et al.* Time-Domain Measurements of Nanomagnet Dynamics Driven by Spin-Transfer Torques. *Science* **307**, 228–231 (2005).
14. Weisheit, M. *et al.* Electric Field–Induced Modification of Magnetism in Thin-Film Ferromagnets. *Science* **315**, 349 (2007).
15. Maruyama, T. *et al.* Large voltage-induced magnetic anisotropy change in a few atomic layers of iron. *Nat. Nano.* **4**, 158 (2009).
16. Weller, D. *et al.* High Ku Materials Approach to 100 Gbits/in^2. *IEEE Trans. Magn.* **36**, 10–15 (2000).
17. Ikeda, S. *et al.* A perpendicular-anisotropy CoFeB–MgO magnetic tunnel junction. *Nat. Mater.* **9**, 721–724 (2010).
18. Winterlik, J. *et al.* Design Scheme of New Tetragonal Heusler Compounds for Spin-Transfer Torque Applications and its Experimental Realization. *Adv. Mater.* **24**, 6283–6287 (2012).
19. Mizukami, S. *et al.* Long-Lived Ultrafast Spin Precession in Manganese Alloys Films with a Large Perpendicular Magnetic Anisotropy. *Phys. Rev. Lett.* **106**, 117201 (2011).
20. Kurt, H. *et al* High spin polarization in epitaxial films of ferrimagnetic Mn_3Ga. *Phys. Rev. B* **83**, 020405(R) (2011).
21. Puntes, V. F. *et al.* Collective behaviour in two-dimensional cobalt nanoparticle assemblies observed by magnetic force microscopy. *Nat. Mater.* **3**, 263–268 (2004).
22. Albrecht, M. *et al.* Magnetic multilayers on nanospheres. *Nat. Mater.* **4**, 203–206 (2005).
23. Galanakis, I. *et al.* Defects in CrAs and related compounds as a route to half-metallic ferrimagnetism. *Phys. Rev. B* **74**, 140408(R) (2006).
24. Hellwig, O. *et al.* A new phase diagram for layered antiferromagnetic films. *Nat. Mater.* **2**, 112–116 (2003).
25. Rößler, U. K. & Bogdanov, A. N. Synthetic metamagnetism – magnetic switching of perpendicular antiferromagnetic superlattices. *J. Magn. Magn. Mater.* **269**, L287–L291 (2004).
26. LePage, J. G. & Camley, R. E. Spin-wave spectrum of a superlattice with antiferromagnetic interfacial coupling. *Phys. Rev. B* **8**, 9113–9121 (1989).
27. Lauhoff, G. *et al.* Ferrimagnetic τ-MnAl/Co Superlattices on GaAs. *Phys. Rev. Lett.* **79**, 5290–5293 (1997).
28. Qiu, R. *et al.* Magnon energy gap and the magnetically structural symmetry in a three-layer ferrimagnetic superlattice. *phys. stat. sol. (b)* **243**, 1983–1995 (2006).
29. Velthuis, S. G. E. *et al.* Spin Flop Transition in a Finite Antiferromagnetic Superlattice: Evolution of the Magnetic Structure. *Phys. Rev. Lett.* **89**, 127203 (2002).
30. Lauter-Pasyuk, V. *et al.* Transverse and Lateral Structure of the Spin-Flop Phase in Fe/Cr Antiferromagnetic Superlattices. *Phys. Rev. Lett.* **89**, 167203 (2002).
31. Stanciu, C. D. *et al.* All-Optical Magnetic Recording with Circularly Polarized Light. *Phys. Rev. Lett.* **99**, 047601 (2007).
32. Alebrand, S. *et al.* Light-induced magnetization reversal of high-anisotropy TbCo alloy films. *Appl. Phys. Lett.* **101**, 162408 (2012).
33. Mangin, S. *et al.* Engineered materials for all-optical helicity-dependent magnetic switching. *Nat. Mater.* **13**, 286–192 (2014).
34. Stanciu, C. D. *et al.* Subpicosecond Magnetization Reversal across Ferrimagnetic Compensation Points. *Phys. Rev. Lett.* **99,** 217204 (2007).
35. Ostler, T. A. *et al.* Ultrafast heating as a sufficient stimulus for magnetization reversal in a ferrimagnet. *Nat. Commun.* **3**, 666 (2012).
36. Piramanayagam, S. N. *et al.* Magnetic and First-Order Reversal Curve Investigations of Antiferromagnetically Coupled Nanostructures of Co/Pd Multilayers. *IEEE Trans. Magn.* **48**, 3410–3413 (2012).
37. Deng, S. *et al.* Magnetostatic Interactions in Antiferromagnetically Coupled Patterned Media. *J. Nano. Nano.* **11**, 2555–2559 (2011).
38. Galanakis, I., Dederichs, P. H. & Papanikolaou, N. Slater-Pauling behavior and origin of the half-metallicity of the full-Heusler alloys. *Phys. Rev. B* **66**, 174429 (2002).
39. Coey, J. M. D. *Magnetism and Magnetic Materials* (Cambridge University Press, Cambridge, , England, 2010).
40. Zhu, L. *et al.* Multifunctional $L1_0$-$Mn_{1.5}Ga$ Films with Ultrahigh Coercivity, Giant Perpendicular Magnetocrystalline Anisotropy and Large Magnetic Energy Product. *Adv. Mater.* **24**, 4547–4551 (2012).
41. Li, M. *et al.* Strong dependence of the tetragonal Mn2.1Ga thin film crystallization temperature window on seed layer. *Appl. Phys. Lett.* **103**, 032410 (2013).

42. Lu, E. *et al.* Reconstruction Control of Magnetic Properties during Epitaxial Growth of Ferromagnetic $Mn_{3-\delta}Ga$ onWurtzite GaN(0001). *Phys. Rev. Lett.* **97**, 146101 (2006).
43. Ma, Q. L. *et al.* Abrupt Transition from Ferromagnetic to Antiferromagnetic of Interfacial Exchange in Perpendicularly Magnetized $L1_0$-MnGa/FeCo Tuned by Fermi Level Position. *Phys. Rev. Lett.* **112**, 157202 (2014).

Achnowledgement

This work was partially supported by the Strategic Japanese-German Cooperative Program ASPIMATT (JST), a Grant-in-Aid for Scientific Research (No. 24686001), and the Asahi Glass Foundation.

Author contributions

Q.M. conceived the idea and designed the experiments. Q.M. fabricated and measured the samples with the help of S.M. Q.M., S.M., X.Z., and T.M. discussed the results. Q.M. anlysed the results and wroted the manuscript with the help of all authors. The study was performed under the supervision of S.M. and T.M.

Additional information

Supplementary information accompanies this paper at http://www.nature.com/scientificreports

Competing financial interests: The authors declare no competing financial interests.

How to cite this article: Ma, Q.L., Zhang, X.M., Miyazaki, T. & Mizukami, S. Artificially engineered Heusler ferrimagnetic superlattice exhibiting perpendicular magnetic anisotropy. *Sci. Rep.* **5**, 7863; DOI:10.1038/srep07863 (2015).